L'GARDE
SMART SPACE TECHNOLOGY

L • GARDE INC. CORPORATE PRESENTATION

On-Orbit Shape Correction of Inflatable Structures

M. Salama, C.P. Kuo, J. Garba, B. Wada

ON-ORBIT SHAPE CORRECTION OF INFLATABLE STRUCTURES*

M. Salama, C.P. Kuo, J. Garba, B. Wada
Jet Propulsion Laboratory
California Institute of Technology
Pasadena, CA. 91109

M. Thomas
L'Garde, Inc.
Tustin, CA. 92680

ABSTRACT

Piezo induced deformations are proposed as a means of achieving a higher degree of on-orbit surface accuracy of inflatable antennas. A series of tests were performed on an inflated circular membrane and an inflated tube, both made of off-the-shelf piezo film. The same configurations were also analyzed to validate the tests. The concept was demonstrated qualitatively in spite of a discrepancy between the analysis and test results, most likely due to inaccurate knowledge of the piezoelectric coefficients of the film.

Numerical simulations are also reported herein, which demonstrate the piezocontrol of an antenna design concept. A parametric study is carried out to determine the most effective distribution of actuators and their optimal gains required to correct given aberrations in the surface of the antenna. The proposed approach is generally suitable for making small local adjustments in the shape of the antenna.

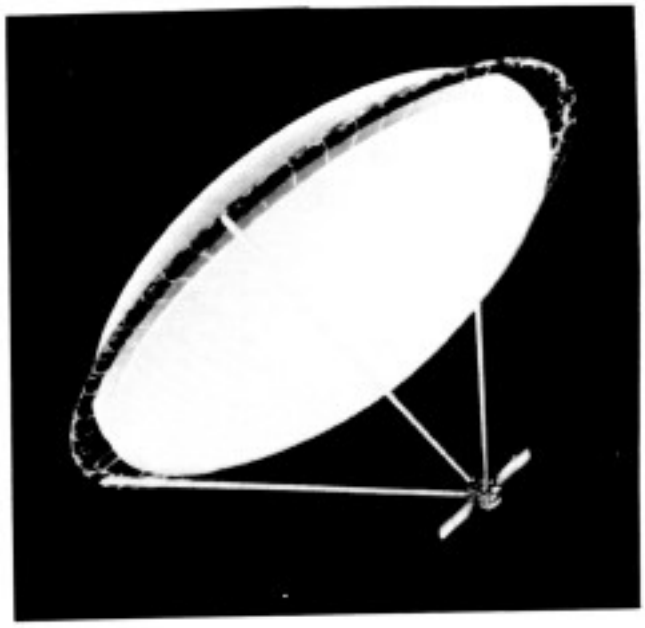

Figure 1: An Inflatable Antenna Concept

I. Introduction:

By comparison to mechanically erectable systems, inflatable structures have been shown[1] to have the advantage of a much lower cost, weight, and packaging volume, as well as more favorable thermal gradients and damping characteristics. The use of inflatable concepts for emergency slides in aircrafts or airbags in cars is an evidence of their deployment reliability. In space applications, an airbag system is currently under consideration as a means of attenuating the landing impact of NASA's MESUR pathfinder spacecraft on the surface of Mars. The use of such technology in the construction of large, lightweight, yet precisely shaped antennas and reflectors can make many important space missions practical.

The precision inflatable antenna in Fig. (1) is an example of a large lightweight antenna concept. Depending on the application, inflatable antennas or reflectors can be made to work at frequencies as high as 3 GHz (radiometry), or 100 GHz (communications). Reference [2] shows that during ground tests, surface deviations from the desired shape of such reflectors are routinely about 1 mm rms. To go to higher frequencies will require a step increase in the surface accuracy of inflatable reflectors. Once attained, the required level

* The research described in this paper was carried out in part by the Jet Propulsion Laboratory, California Institute of Technology under contract with the National Aeronautics and Space Adminstration.

of accuracy may be maintained by making periodic on-orbit shape adjustments as the antenna is exposed to thermal changes and possible aging of the polymeric film.

The on-orbit adjustment of an inflatable space antenna can be made by several techniques. Varying the inflation pressure can enable substantial adjustment of the focal length by making global shape changes [2]. Unfortunately, this will do little to correct unsymmetric distortions. The use of electrostatic charge to change the shape of a deployed reflecting membrane has also been examined [3]. The idea was to pull on sections of the deployed membrane by applying a static electric charge to certain regions of an adjacent parallel membrane. The technique was partially successful and was not sufficiently lightweight.

The concept explored in the present paper offers a potentially lightweight and simple technique to correct local aberrations in the shape of an inflated membrane by shrinking or stretching sections of the membrane or support structure. This can be done by employing piezoelectric elements in the construction of the membrane or support structure. The piezoelectric element may be a thin polymeric film, much similar to that normally used for the inflatable membrane itself. A positive or negative electric field applied to the piezofilm creates a mechanical strain proportional to that field. This provides the ability to induce controlled on-orbit dimensional changes in gores of the antenna itself or its attachments in order to optimize the reflector performance. The technique is suitable, not for making large focal length changes, but for making small symmetric or unsymmetric local adjustments. As such it could complement the variable pressure approach of Ref. [2]. Some theoretical aspects of the present technique has been examined in an earlier paper [4]. Its feasibility is further explored in the present paper by a combination of laboratory experiments and numerical simulations using simple configurations, as well as numerical simulations and trade studies using the more realistic design concept of Fig. (1).

II. Actuated Inflatables:

The ability to make small shape corrections in an inflated structure is considered here by integrating the actuation mechanism in the inflated membrane itself or in its support structure. Since in most cases the support structure is likely to be also an inflatable membrane, this section will deal with distributed piezoelectric actuation of membranes.

1. Distributed **Piezoelectric** Actuation: The phenomenon of piezoelectricity couples the electrical and mechanical properties of certain materials. Polymers, for example, are comprised of many randomly oriented positive and negative dipoles. Their piezo property can be induced through a one-time application of a sufficiently high voltage at high temperature, which results in permanent polarization of the dipoles. The process, called "poling", locks in the piezoelectric effect anisotropically, along and normal to the poling direction. Once poled, the strains will depend not only on the applied stress, but also on the applied electric field and dielectric displacement. The coupled electromechanical constitutive relations then take the general form [5]:

$$D_k = d^T_{k\ell m}\sigma_{\ell m} + \eta^{\sigma}_{kn}{}^T E_n$$
$$\epsilon_{ij} = s^{E}_{ij\ell m}{}^{T}\sigma_{\ell m} + d^T_{ijn}E_n \qquad (1)$$

The first equation describes the "direct" piezoelectric effect and states that the dielectric displacement vector D depends upon the stress tensor σ and electric field E through the piezoelectric coefficient matrix d and the permittivities η, respectively. On the other hand, the second equation describes the "converse" piezoelectric effect and states that in presence of an electric field E, the strain tensor ϵ depends upon the applied stress tensor σ as well as the electric field through the elastic compliance s and the piezoelectric coefficients d, respectively. In both equations, the superscript T indicates transpose. Other superscripts indicate that the coefficient in question is evaluated at a constant value of the superscript.

In polymeric films, piezoelectricity is introduced by poling in the "3"-direction. This is the direction of the normal to the plane of the film. By constructing an inflatable component from this piezoelectric film, a subsequent application of voltage to the film will induce a distributed in-plane actuation strain field in addition to the existing strains due to inflation pressure. From the second of Eq. (1), the components of strain at a point in the film are then obtained from:

$$\epsilon_{11} = s_{11}\sigma_{11} + s_{12}\sigma_{22} + d_{31}E_3$$
$$\epsilon_{22} = s_{22}\sigma_{22} + s_{12}\sigma_{11} + d_{32}E_3$$
$$\epsilon_{12} = s_{44}\sigma_{12} + d_{14}E_2 \qquad (2)$$

Thus, the in-plane piezoelectric constants d_{31}, d_{32} are exploited in inflated membranes as a means of inducing a desired state of in-plane membrane strains, sufficient to correct a prescribed amount of out-of-plane deformations. The d_{31}, d_{32} constants describe the strains in

the in-plane directions "1" and "2", respectively, when an electrical field is applied in the thickness direction "3". In the presnt application, $E_2 = 0$.

Piezoelectric films are now commercially available off-the-shelf. They are typically employed as sensors in devices for a wide variety of applications, e.g. pressure sensors. Their use in distributed sensing and control has been investigated only recently [6]. The piezo film used here is a polyvinylidene fluoride semicrystalline resin (a.k.a. PVDF), known by the trade name Kynar. The film comes in various thicknesses, with a very thin metal layer deposited on each side to provide electrical connection.

2. Experiments: The purpose of the laboratory experiments that follow is to explore the advantages and limitations of these films as inflatables with built-in distributed actuation ability, suitable for correcting shape aberrations. The test configurations are kept simple to minimize costs and test variables. Thus instead of the relatively complex inflatable structure of Fig. (I), the actuation ability of piezoelectric films was explored experimentally on the inflated circular membrane and closed tube configurations in Fig. (2).

Figure (2a) shows two circular membranes, initially flat and rigidly clamped along their 10. in diameter boundary. Inflation pressure is introduced in the air space between the two membranes. Because of the rigid boundary conditions, each membrane deforms under pressure independent from the other. As a check on the test/analysis results (to be discussed later), one membrane was chosen to be 0.001 in mylar (isotropic), and the other a 0.002 in Kynar membrane (anisotropic), comprised of approximately 0.0015 *in* basic PVDF film, on which two layers (.0005 in total thickness) of silver ink metallization are deposited (one layer on each side for electric contact). As the inflation pressure is changed, the deformed shape of each membrane relative to the flat undeformed configuration is monitored at the center and four other points on each membrane. Up to 0.5 psi internal pressure was applied, and the corresponding lateral deformations (up to 0.5 in) were measured using dial gage type sensors. When up to 300 volts were applied to the pressurized Kynar membrane, additional lateral membrane deformations of the order of 0.001 *in* were recorded using eddy current sensors.

The tube in Fig. (2b) is made of the same 0.002 in Kynar membrane with the "1"-axis parallel to the tube axis (i.e. d_{31} is along the longitudinal direction). Separate strips of conducting piezo are created by chem-

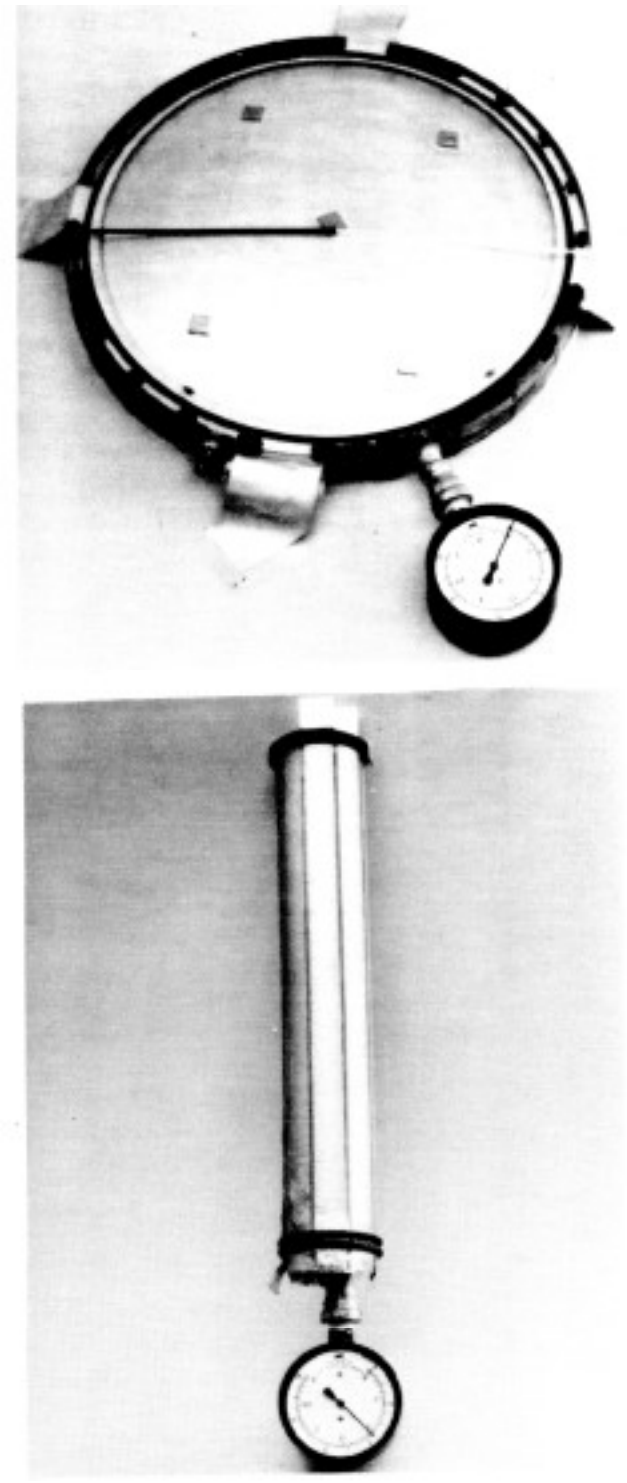

Figure 2: Piezoelectric Actuated Test Components (a) Circular Membrane, (b) Tube

ically etching thin strips of the metallization on both sides of the film. The tube is closed at each end with a 1/2 *in* plastic disk. During the experiment, the bottom end of the tube is rigidly fixed and the deformations at the top free end are monitored in three directions as the inflation pressure (up to 1.0 *psi*) is applied, separately or in addition to electric fields applied individually to the metallized strips.

III. Analysis/Test Results:

Analysis was also performed to corroborate the results of tests described above, and to examine the applicability of the concept to more practical configurations. Consistent with the fact that the stiffness of inflatable structures is largely dependent upon the internal pressure, the analysis method assumes large elastic deformations with small membrane strains. For this purpose, the nonlinear finite element analysis capability in NASTRAN was found to be sufficiently accurate.

1. Inflation Pressure Only: In Fig. (3), the test center deformation on the mylar side of the circular membrane (Fig. 2a) is compared to two independent analysis methods; NASTRAN's nonlinear analysis, and the series solution of Ref. [7]. Both methods of analysis give almost identical results, which tend to be approximately 10% stiffer than the test results. Inaccuracy in the mylar's elastic modulus value used in both analyses (0.5375 x 10^6 *psi*), is the most likely reason for the discrepancy.

2. Piezoelectric Actuation: In the piezo actuated tests, the Kynar membrane in Fig. (2a) is first inflated then subjected to an electric field through the leads. The applied voltage was varied from zero to 300 volts, and from zero to -390 volts. A series of such tests was performed at different inflation pressures (p_i = 0.1, 0.2, 0.3, 0.4, *and* 0.5 *psi*). The deformed membrane surface Δ_{pi} at pressure p_i is used as a reference, from which additional deformations δ^v_{pi} due to the applied voltage are measured. Figures (4a, 4b) together show typical results for inflation pressure p_i = 0.2 *psi*, in the form of applied voltage and corresponding deformations at the center and four other locations indicated in Fig. (2a). As seen from Fig. (4), the hysteresis is elastic and recoverable. Here, positive voltage induces negative strain (shrinkage), and negative voltage induces positive strain (stretching).

As a measure of the rate of deformation per volt for the present test configuration, the average slope of the hysteretic curve for the center deformation was computed. For inflation pressures ranging from 0.1 *psi* to 0.5 *psi*, the average rate was found to range from 4.1 x 10^{-6} to 3.6 x 10^{-6} in/volt. Larger rate corresponds to lower inflation pressure. These test values are compared bellow to the analysis results.

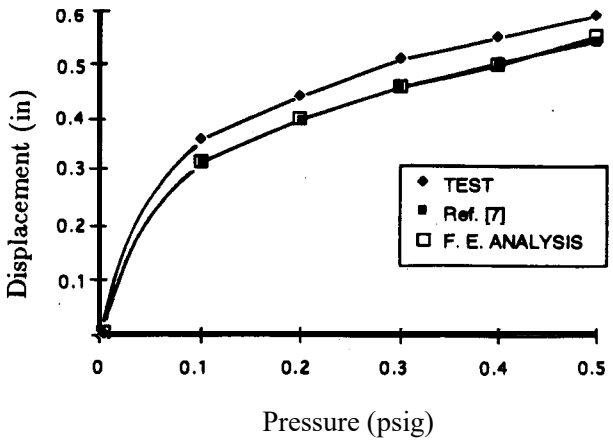

Figure 3: Analysis/Test Comparison of Inflated Circular Membrane

Referring to Eq. (2), one observes that the piezoelectic strains, $d_{31}E_3$ and $d_{32}E_3$, behave numerically analogous to thermal strains of the form, $-\alpha_{31}$ AT and $-\alpha_{32}\Delta T$, where AT is the change in temperature, and α_{31}, α_{32} are anisotropic expansion coefficients in directions " 1" and "2", respectively. This analogy was exploited in the numerical simulation of the piezo actuated inflated membrane. Thus in NASTRAN's nonlinear analysis simulations, large membrane deformations are computed iteratively under a simultaneously applied inflation pressure p_i and temperature change AT, the magnitude of which is chosen such that;

$$d_{31}E_3 = \alpha_{31}\Delta T, \quad and \quad d_{32}E_3 = \alpha_{32}\Delta T \qquad (3)$$

The following values were used in Eq. (3) and the analysis: $d_{31} = 0.9 \times 10^{-9}$ *in/in/volt/in*, $d_{32} = 0.117 \times 10^{-9}$ *in/in/volt/in*, Elastic modulus= 0.29 x 10^6 psi, α_{31} = 28.0 x 10^{-6} *in/in/F°*, and α_{32} = 4.0 x 10^{-6} *in/in/F°*. Note that both d_{31}, d_{32} should be divided by the membrane thickness before their use in Eq. (3). For comparison with the test results in Fig (4), the rate of center deformation per volt was computed from the analysis and were found to range from 13.9 x 10^{-6}*in/volt* to 8.2 x 10^{-6}*in/volt* for inflation pressures ranging from 0.1 *psi* to 0.5 psi. Considering the good analysis/test correlation in Fig. (3), the discrepancy of about a factor of three may be due to

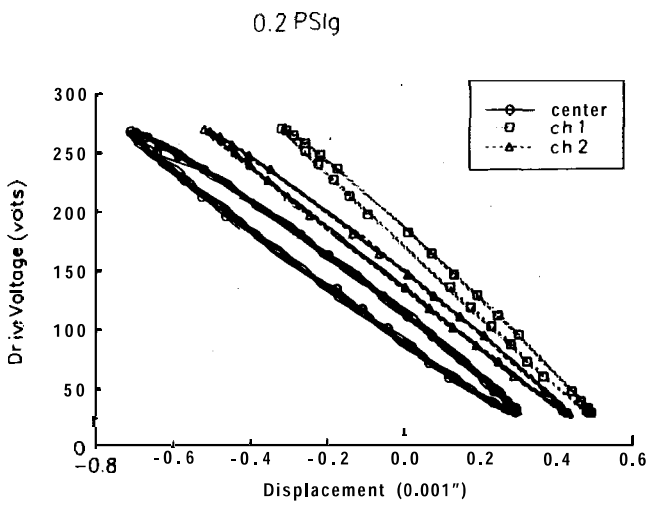

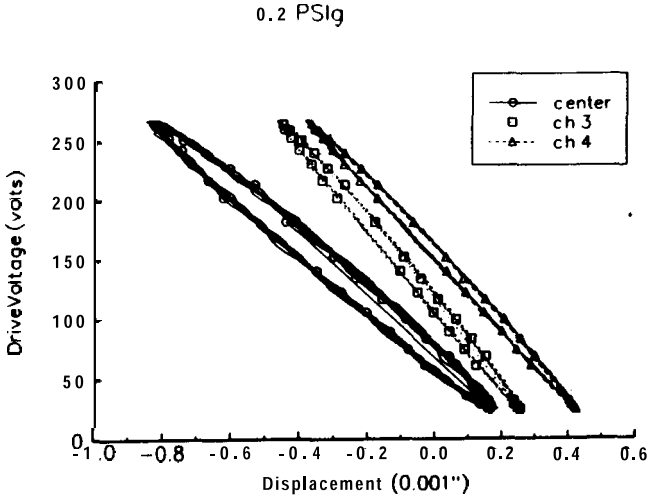

Figure 4: Piezoactuated Deformation of Inflated Circular Membrane At Center and Points Marked in Fig. 2a.

inaccuracies in values of the material constants listed above. According to the manufacturer, measurement of d_{33} can be made much more accurately than for d_{31}, d_{32}.

As in the circular membrane, piezo actuation tests of the tube in Fig. (2b) were performed by applying voltage to the leads of the already inflated tube, with the bottom end rigidly **fixed.** To simulate line-of-sight adjustments of the free end of the tube relative to the **fixed** end, an equal and opposite voltage was applied to the leads of only two strips on opposite sides of the tube. The deformations δ^{v}_{pi} due to the applied voltage alone are then measured at the three degrees of freedom at the free end. Figure (5) is an example of these

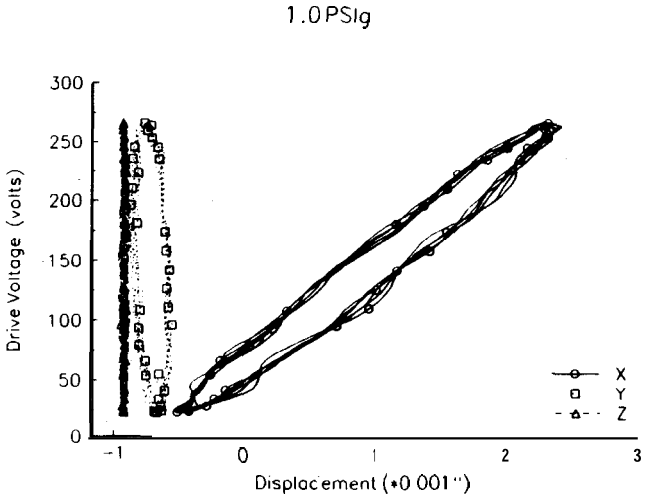

Figure 5: Piezoactuated Deformation At Free End of Inflated **Tube**

measurements at pressure $p_i = 1.0psi$ as the voltage is varied. Here again the deformation rate per volt was computed **from** the test data at the lateral **degree-of-freedom** for $p_i =$ 0.5, **,0.6,** 0.7, 0.8, 0.9, ***and*1.0** psi and **was** found to range from 12.0 x10^{-6} to 11.1 x10^{-6} in/volt. The analysis followed the same procedure described above for the circular membrane, and discrepancies of the same order (factor of 3) was also encountered for the tube configuration. Figure (6) is an example of the analysis simulation results of the piezo actuated **line-of-sight** adjustment.

IV. **Piezocontrol** of Antenna System:

The antenna system in **Fig.(7)** is a finite element idealization of Fig. (1) without the tripod. The **axisymmetric** parabolic antenna membrane has a diameter $D = 120.0in$, $F/D = 0.5$, thickness = 0.00025 in, and is **inflated** and taut at the outer edge by 16 **tie-rods** to a thin-walled torus. The nominal dimensions of the tie-rods are: length $= 6.0in$, area $= 0.03in^2$, and those of the torus are: radius of centerline $= 72.0in$, tube radius $d_t = 6.0in$, **and** thickness $t_t = 0.02in$. The surface accuracy of the inflated parabolic antenna depends upon several parameters such as the initial uninflated shape, inflation pressure, edge conditions at the torus interface, **elastic** interaction between the parabolic membrane and the supporting torus, imperfections in the fabrication process of any of the above components, and the operating conditions in space. On-orbit correction of deviations from the desired shape can be implemented by several piezo actuation methods. These are discussed next.

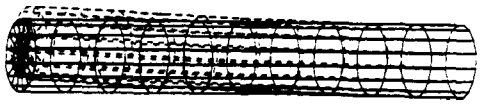

Figure 6: Simulation of Piezoactuated Line-of-sight

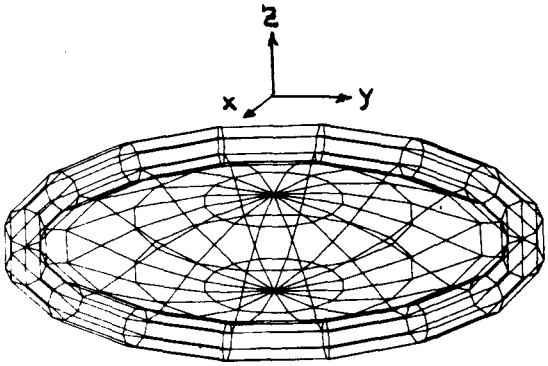

Figure 7: Finite Element Idealization of Inflated Parabolic Antenna/Torus System

1. Simulations: In the following simulation scenario, we assume that aberrations in the antenna surface are the result of out-of-plane circumferential sinusoidal distortion of the torus centerline from the XY-plane in the form: $d_z = d_o sin3\theta$, with zero values at the three interface points to the supporting tripod. Such imperfection in the torus will give rise to a deformed state, u^d, of the inflated antenna which differ from the deformed state, u^o, had the torus been perfect. Then the vector of aberrations we wish to correct is taken to be: $u^* = (u^d - u^o)$. Only deformation components in the Z-direction (parallel to axis of symmetry) at the nodes on the parabolic membrane are included in u^*.

One approach to **correct the aberrations u^* on-orbit is by introducing controlled amounts of piezo actuated strains along axes of the tie-rods.** To achieve the best correction, the actuation gain (magnitude of voltage or displacement induced in each tie-rod) must be optimally distributed among the tie-rods.

Let n_c = number of degrees of freedom in the controlled set u^*, and n_{ap} = number of possible actuators (here 16 tie-rods). Also let:

$\tilde{S} = (n_c \times n_{ap})$ matrix of influence coefficients, each column of which represents the deformation state at the n_c control d.o.f due to a unit actuation gain at one actuator location,

$\Delta_o = (n_{ap} \times 1)$ vector of unknown actuator gains,

Then, the deformations u at the same n_c controlled d.o.f. due to applying a combination of actuation gains Δ_o at the tie-rods is:

$$u = \tilde{S}\Delta_o \tag{4}$$

Now the unknown gains Δ_o may be determined optimally in a least square sense by requiring, $u^* - u = 0$, so that;

$$\Delta_o = (\tilde{S}^T\tilde{S})^{-1}\tilde{S}^T u^* \tag{5}$$

In general, it may be desirable to use fewer actuators n_a than the total number of possible actuator locations n_{ap}. In this case, the actuator locations should be also selected optimally. Since the actuator locations are discrete variables, a discrete optimization technique such as the simulated annealing algorithm [8] may be used for selecting the optimal actuator locations and gains. The algorithm is iterative. It does not require gradient information, and is designed to avoid getting trapped in local minima. During a typical kth iteration, the algorithm selects n_a out of all possible n_{ap} actuator locations. Let,

$J_k^*(j)$ = the integer vector of n_a location indices $j = 1,\ldots,n_a$, such that $J_k^*(j) \in n_{ap}$ specifies the n_a locations selected during the current simulated annealing iteration, and

$B_k = (n_{ap} \times n_a)$ location selection matrix, whose b_{ij} elements are either "one" or "zero" depending upon whether or not $i = J_k^*(j)$ for any j and for $i = 1,\ldots,n_{ap}$.

Then, analogous to Eqs. (4,5);

$$u_k = S_k\Delta_{ok}$$

$$S_k = \tilde{S}B_k$$

$$\Delta_{ok} = (S_k^T S_k)^{-1}S_k^T u^* \tag{6}$$

As a measure of the proximity of u_k *to* u^*, the algorithm seeks the best actuator locations $J_k^*(j)$ with optimal gains $\Delta_{ok}(j)$, $j = 1, \ldots n_a$ which minimize the normalized rmz error:

$$e_{min} \equiv e_k = \left[\frac{(u^* - S_k\Delta_{ok})^T(u^* - S_k\Delta_{ok})}{u^{*T}u^*}\right]^{1/2} \quad (7)$$

2. Analysis **Results:** Results of the numerical implementation of the methodology described above are given here for different cases that differ in the number of d.o.f. included in the control set u^*, and in the number of 'actuators used to perform the shape adjustment. For all cases, the rms of the control d.o.f. in u^* is 1.28 x 10^{-3} in. Table 1 summarizes the optimization results when the number of control d.o.f in the u^* set are $n_c =$ 17, 25, and 49. The specific choice of members of these sets is shown in Fig. (8), and was made to represent progressively finer granularity in the number of sensors one may use in monitoring the shape of the antenna. Notice that the intentional choice of $n_c(17) \in n_c(25) \in n_c(49)$, does not guarantee that the resulting optimal locations (see Table 1) satisfy the same relation, $n_a(4) \in n_a(8) \in n_a(16)$.

The effect of increasing the number of control d.o.f. n_c to be monitored and the number of actuators n_a on the ability to adjust the antenna errors is shown in Table 1 and Fig. (9). As one may expect, more accurate adjustment is possible as more actuators are brought to share in the process, and as one tries to enforce the adjustment at a fewer number of d.o.f. Conversely, the accuracy deteriorates as one tries to use the same number of actuators to enforce adjustment of shape at a larger number of d.o.f. The ideal situation is when the number of actuators and number of control d.o.f. are equal, $n_a = n_c$, in which case exact adjustment of the shape is assured. It should be realized, however, that achieving higher degree of adjustment accuracy at the d.o.f. included in u^* **does** not guarantee equally high accuracy at d.o.f. excluded from u^*. The latter may become even worse. It is important, therefore, that the control d.o.f. be selected judiciously.

Rather than volts, the optimal actuator gains in Table 1 represent **displacements** (or travel) which the actuators must provide. The use of piezo films to provide this level of displacement in the tie-rods would require their redesign. However, off-the-shelf **PZT** ceramic actuators are usually capable of up to 4 x10^{-3} in travel. Thus, except for the case when, $n_a = 16$, $n_c =$ 17, one could use existing PZT ceramic actuators. Otherwise, the actuator design must be modified for specific applications. Of course, design limitations will have to be imposed on their energy consumption and weight.

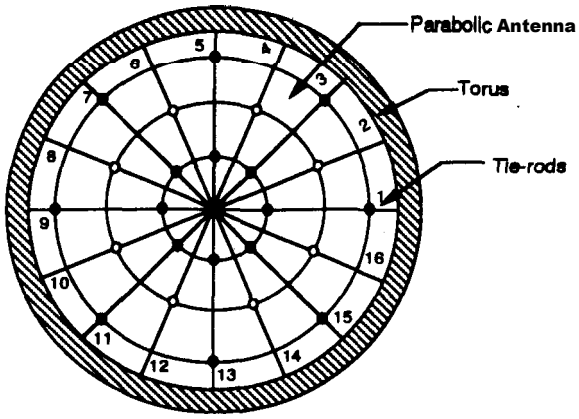

Figure 8: Control d.o.f. and Tie-rod Locations
$n_c = 17$: "●"
$n_c = 25$: "●+o"
$n_c = 49$: All Z-d.o.f. on Antenna

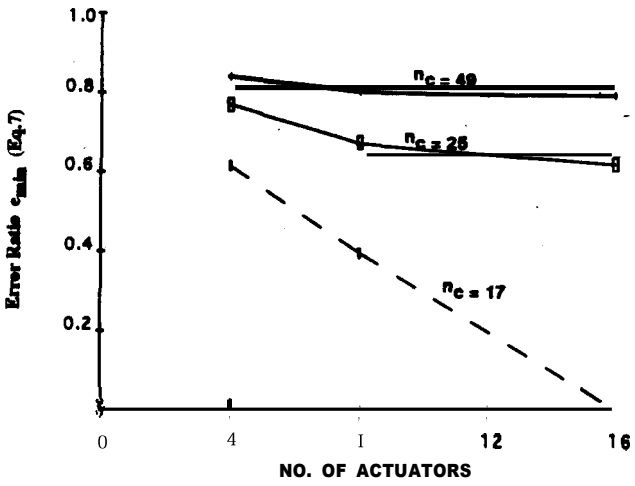

Figure 9: Error Ratio e_{min} As Function of n_a, n_c

3. Other Actuation schemes: Rather than inducing piezo strains in the tie-rods to correct the aberrations in the inflated membrane, another approach may be to **induce the piezo strain directly in sectors (gores) of the parabolic membrane.** This would be similar the experiments discussed in **Sec.** II. Electric separation of the **different** sectors or regions is easily achieved by chemical etching of the metallization. This approach **has** the advantage of increasing the number of possible actuation regions, n_a, thereby reducing the required **voltage.**

A third approach involves application of **piezoelectric** moments locally at different locations along the circumference of the torus. Such moments would **cor-**

rect distortions in the torus directly. This scheme was attempted on the system of Fig. (7), but was abandoned because it required too high voltage to deform the relatively very stiff torus.

V. Concluding Remarks:

The concept of using induced piezo strains to control on-orbit dimensional changes in elements of inflatable structures was investigated here analytically and experimentally. Off-the-shelf material was used to construct relatively simple laboratory experiments. Feasibility of the approach was demonstrated qualitatively. However, due to inaccurate knowledge of the anisotropic piezoelectric coefficients of the piezo film, a factor of three discrepancy was found between the analysis and test results. More accurate characterization of these constants is required.

For a 10.0 in diameter, 0.002 in thick membrane, out-of-plane center deformation of about 0.0012 in was obtained during the experiment when about 300 volts were applied. One would expect this deformation to scale directly with diameter. Thus, the demonstrated piezo induced deformations would be of the order 0.05 in for 14-meter diameter F/l system, such as the inflatable reflector to be flown on the Inflatable Antenna Experiment of Ref. [9]. Manufacturing tolerances have been shown to cause focal length changes on the order of several inches for a 14-meter diameter antenna. So, the demonstrated piezo approach would not be appropriate for this level adjustments. On the other hand,

Table 1: Optimized Performance of Antenna System As Function of n_a, n_c. (Gain $\times 10^{-3} in$)

No. of Actuators	e_{min}	n_c = 17 Actuator No.	Gain	e_{min}	= 25 uator lo.	Gain	e min	= 49 Actuator No.	Gain
n_a = 4	0.612	1	-4.4	0.766	6	-1.3	0.837	6	-1.1
		5	2.7		9	-1.0		9	-2.1
		7	4.2		12	-2.6		11	-0.9
		12	-3.8		14	-2.4		12	-1.7
n_a = 8	0.395	4	-2.6	0.671	1	-0.5	0.800	1	-0.7
		5	2.6		6	-2.6		3	a.9
		7	3.9		7	1.3		6	-1.2
		8	-2.4		9	-1.6		,	1.1
		10	-1.8		10	1.1		9	-2.2
		11	3.0		11	0.6		10	0.9
		13	2.9		12	-2.6		11	0.9
		14	-3.3		14	-2.1		12	-1.4
n_a = 16	~0.0	1	-16.1	0.619	1	-0.5	0.792	1	-0.7
		2	4.9		1	1.5		1	0.3
		3	-6.6		3	-0.3		3	-0.6
		4	-0.7		.	-1.0		.	-0.1
		5	8.5		5	0.4		9	0.1
		6	11.8		6	-3.0		6	-1.2
		7	12.1		7	0.1		7	0.9
		8	-6.8		8	1.5		6	0.9
		9	0.9		9	-1.5		9	-2.1
		10	-7.4		10	1.6		10	0.9
		11	13.2		11	0.6		11	0.9
		12	20.2		12	-3.1		12	-1.3
		13	6.3		13	0.6		13	0.0
		14	-20.3		14	-2.4		14	-0.3
		15	-18.4		15	0.3		15	-0.1
		16	-5.8		16	1.1		16	0.21

small adjustments in the gore lengths or tie-rods may be sufficient to correct symmetric or unsymmetric local irregularities in the membrane surface arising from material imperfections, modulus variations, or other causes of small dimensional instabilities. The combination of a pressure control to adjust the focal length, and piezoelectric control to reduce deviations from the desired shape, could provide the added increase in surface accuracy needed to extend the use of inflatable antennas into the high frequency domain.

References:

1 Thomas, M. and G.F. Friese, "Pressurized Antennas for Space Radars," AIAA Sensor Systems for the 80's Conference, CP807, December 1980.

2. Thomas, M. and Veal, G.; "Scaling Characteristics of Inflatable Paraboloid Concentrators," ASME Solar Engineering, Ed.: Mancini, T., Watanabe, K., and Klett, D., 1991, pp. 353-358.

3. Goslee, J.W., "Progress Report on the Electrostatic Membrane Antenna Concept Testing," - Large Space Systems Technology Conference, 1981, NASA Conference Publication 2215, part 2, 1981, pp. 681-687.

4. Utku, S., Kuo, C.P., Garba, J., Salama, M., and Wada, B., "Adaptive Inflatable Space Structures: Shape Control of Reflector Surface," 4th International Conference on Adaptive Structures, Maternushaus, Cologne, Germany, November 1993.

5. Jaffe, B., Cook, W., and Jaffe, H., Piezoelectric Ceramics, Academic Press Limited, 1971.

6. Tzou, H.S., Piezoelectric Shells: Distributed Sensing and Control of Continua, Kluwer Academic Publishers, 1993.

7. Hencky, H., "Uber den Spannungszustand inkreisrunder Platten mit verschwindender Biegungssteifigkeit," Zeits. Math. Phys., Vol. 63, 1915, pp. 311-316.

8. Chen, G-S., Bruno, R., Salama, M., "Optimal Placement of Active / Passive Members in Truss Structures Using Simulated Annealing," AIAA J., Vol. 29, 1991, pp. 1327-1334.

9. Freeland, HE., Bilyeu, G.D., Veal, G.R., "Validation of a Unique Concept for a Low Cost Lightweight Space Deployable Antenna Structure," 44th Congress of the International Astronautical Federation, October 1993, paper No. IAF-93-I.1.201.

L•Garde Inc
15181 Woodlawn Avenue
Tustin, CA 92780-6487
www.LGarde.com